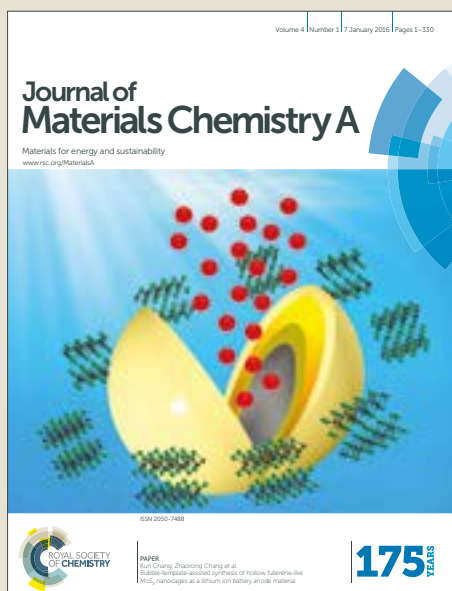


# Journal of Materials Chemistry A

Accepted Manuscript



This article can be cited before page numbers have been issued, to do this please use: Z. Zhou, Z. Wu, Q. Xu and G. Zhao, *J. Mater. Chem. A*, 2017, DOI: 10.1039/C7TA08112J.

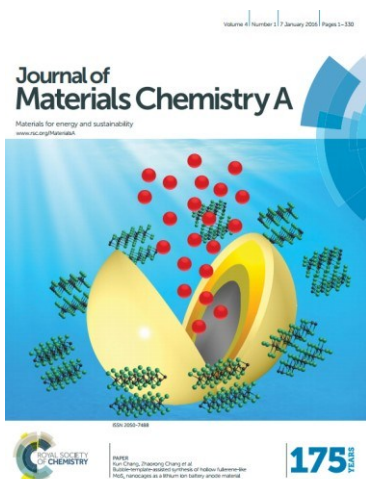


This is an Accepted Manuscript, which has been through the Royal Society of Chemistry peer review process and has been accepted for publication.

Accepted Manuscripts are published online shortly after acceptance, before technical editing, formatting and proof reading. Using this free service, authors can make their results available to the community, in citable form, before we publish the edited article. We will replace this Accepted Manuscript with the edited and formatted Advance Article as soon as it is available.

You can find more information about Accepted Manuscripts in the [author guidelines](#).

Please note that technical editing may introduce minor changes to the text and/or graphics, which may alter content. The journal's standard [Terms & Conditions](#) and the ethical guidelines, outlined in our [author and reviewer resource centre](#), still apply. In no event shall the Royal Society of Chemistry be held responsible for any errors or omissions in this Accepted Manuscript or any consequences arising from the use of any information it contains.



# Journal of Materials Chemistry A

## Materials for Energy and Sustainability

Full paper submission

*Journal of Materials Chemistry A* is a weekly journal in the materials field. The journal is interdisciplinary, publishing work of international significance on all aspects of materials chemistry related to energy and sustainability. Articles cover the fabrication, properties and applications of materials.

2016 Impact Factor of *Journal of Materials Chemistry A*: **8.867**  
For more information go to [www.rsc.org/materialsA](http://www.rsc.org/materialsA)

The following paper has been submitted to *Journal of Materials Chemistry A* for consideration as a **Full paper**.

The Editorial Board stress a **very high quality and novelty** standard is needed for acceptance.

*Journal of Materials Chemistry A* wishes to publish original research that demonstrates significant **novelty and advance**, either in the chemistry used to produce materials or in the properties/applications of the materials produced. Work submitted that is outside of these criteria will not usually be considered for publication. The materials should also be related to the theme of materials for energy and sustainability.

We ask referees to examine manuscripts very carefully, and recommend rejection of articles which do not meet our high novelty, quality and impact expectations. Please note that **the rejection rate for JMCA is currently ~80%** of submitted manuscripts. **Routine or incremental** work, however competently researched and reported, should not be recommended for publication if it does not meet our expectations with regard to novelty and impact.

It is the responsibility of authors to provide fully convincing evidence for the homogeneity and identity of all compounds they claim as new. Evidence of both purity and identity is required to establish that the properties and constants reported are those of the compound with the new structure claimed.

Thank you for your effort in reviewing this submission. It is only through the continued service of referees that we can maintain both the high quality of the publication and the rapid response times to authors. We would greatly appreciate if you could review this paper in **ten days**. Please let us know if that will not be possible.

Once again, we appreciate your time in serving as a reviewer. To acknowledge this, the Royal Society of Chemistry offers a **25% discount** on its books: <http://www.rsc.org/Shop/books/discounts.asp>. Please also consider submitting your next manuscript to *Journal of Materials Chemistry A*.

Best wishes,

Annie Harvey  
Executive Editor, *Journal of Materials Chemistry A*



Journal Name

ARTICLE

## Solar-charged Photoelectrochemical Wastewater Fuel Cell for Efficient and Sustainable Hydrogen Production

Zhaoyu Zhou,<sup>†‡</sup> Zhongyi Wu,<sup>†‡</sup> Qunjie Xu<sup>\*b</sup> and Guohua Zhao<sup>\*a</sup>Received 00th January 20xx,  
Accepted 00th January 20xx

DOI: 10.1039/x0xx00000x

www.rsc.org/

It is of great practical significance to realize the efficient treatment of wastewater and the comprehensive utilization of chemical energy of wastewater. Thus, a WO<sub>3</sub>NFs-C/Cu<sub>2</sub>O NWAs visible-light response dual-photoelectrodes solar-charged photoelectrochemical wastewater fuel cell (scPEWFC) was constructed for efficient hydrogen production based on the promotion of phenol oxidation at the anode. The hydrogen production reaches as high as 93.08 μmol cm<sup>-2</sup> by the photoelectrocatalytic oxidation of phenol (TOC removal rate reached 82.12%) of WO<sub>3</sub>NFs-C/Cu<sub>2</sub>O NWAs under visible light irradiation for 8 h without additional bias, which is 3.02 times higher than that of pure photocatalytic water splitting. The excellent photoelectrochemical performance can be attributed to the less endergonic process of phenol oxidation compared to water oxidation, which indicated that phenol oxidation can promote the hydrogen generation at the cathode. Isotopic labelling experiments show that protons were derived from the splitting of water rather than phenol. Interestingly, the effective combination of photochargeable properties of WO<sub>3</sub> with PEC, the hydrogen production (4 h to produce 7.50 μmol cm<sup>-2</sup>) was still carried out at the cathode under the dark owing to the stored electrons of WO<sub>3</sub> under the light, which realized the ideal effect of full-day and high-efficiency hydrogen production. Besides, the mechanism of scPEWFC operation was investigated in detail. This paper provides a new research idea for scPEWFC wastewater treatment, energy recover, electron storage, and simultaneous full-day hydrogen production.

### Introduction

With industrialization, globalization and manufacturing is expanding at an alarming rate in the past decades, the large amount of organics discharged into the water-body caused serious environmental pollution, especially those low concentrate and highly toxic pollutants in the water seriously threaten human health and social development, so the development highly efficient methods of purifying water pollutants is the focus of research and attention from both industry and academia<sup>1-7</sup>. In fact, the researchers found that wastewater containing high levels of organics and as an excellent electron donor, which can be seen as an ideal available energy source<sup>8-10</sup>. In addition, the traditional wastewater treatment technology, such as activated carbon adsorption, membrane separation, Fenton and ozone oxidation technology<sup>11</sup>, have obtained excellent treatment results. Unfortunately, strategy of re-processing, light utilization was adopted, only the separation, enrichment, degradation and destruction of pollutants, and pollutant degradation

is the main purpose of traditional wastewater treatment methods, which ignored a huge amount of chemical energy in the wastewater. Therefore, it is also a hot issue for how to efficiently process wastewater and to reuse the electrons produced by wastewater oxidation<sup>12</sup>.

Microbial fuel cell (MFC) is a kind of device that utilizes microorganisms to convert chemical energy from organic matter directly into electrical energy, which has wide application prospect in wastewater treatment and new energy development<sup>13-19</sup>. However, due to the relatively low current efficiency, the electrons are difficult to store, thus researchers have switched to produce hydrogen with MFC combined with electrocatalysis or photocatalysis effectively. Photoelectrochemical cell (PEC) and MFC were combined to achieve for electricity or hydrogen generation, using wastewater and solar light as the only energy sources<sup>20</sup>. A self-biased solar-driven microbial photoelectrochemical cell that coupled a bacterial-colonizing bioanode with a semiconductor nanowire cathode to achieve the goal of microbial electricity generation were also reported<sup>21</sup>. However, it's difficult to deal with some persistent and biodegradable organic matter with MFC, such as azo dyes, due to its biological tolerance. In addition, the performance of MFC is still limited by the internal resistance of proton mass transfer and oxygen reduction kinetics. The harsh conditions of microbiological culture, enrichment, training and operating environment, low efficiency of electronic transmission, the complex research mechanism limited MFC actual large-scale application<sup>22-24</sup>.

Photoelectrochemical cell (PEC) provide a powerful means of harnessing solar energy for the production of clean hydrogen fuels

<sup>a</sup> School of Chemical Science and Engineering, Shanghai Key Lab of Chemical Assessment and Sustainability, Tongji University, 1239 Siping Road, Shanghai 200092, China. E-mail: g.zhao@tongji.edu.cn

<sup>b</sup> Shanghai Key Laboratory of Materials Protection and Advanced Materials in Electric Power, Shanghai University of Electric Power, Shanghai 200090, China. E-mail: xuqunjie@shiep.edu.cn

<sup>†</sup> Electronic Supplementary Information (ESI) available: [details of any supplementary information available should be included here]. See DOI:10.1039/x0xx00000x

<sup>‡</sup> These authors are co-first authors and contributed equally to this work.

by photoelectrochemical reactions, without additional energy input<sup>25-27</sup>. The early studies focused on single semiconductor electrode PEC<sup>28</sup>. Subsequently, researchers have proposed Z-Scheme type dual photoelectrode photocatalytic fuel cell (PFC)<sup>29-32</sup>, which was mainly composed of n, p-type semiconductors as the photoanode and photocathode, respectively. The Fermi level of n-type semiconductor was more negative than that of p-type semiconductor, an interior bias can be produced to drive the electrons to combine with the holes of photocathode from the external circuit from photoanode<sup>33</sup>. A visible-light responsive photocatalytic fuel cell was constructed based on WO<sub>3</sub>/W or TiO<sub>2</sub>/Ti photoanode and C/Cu<sub>2</sub>O photocathode for simultaneous wastewater treatment and electricity generation by simulating Z-Scheme system<sup>22,34</sup>. Early research was mainly used to treat wastewater and electricity production, but because of the unstable energy output, so it can't be utilized directly. A solar-driven photocatalytic fuel cell with dual photoelectrode for simultaneous wastewater treatment and hydrogen production was constructed in our previous study<sup>8</sup>. In addition, the influencing factors of PEC such as electrode materials and target pollutants were investigated. The Z-Scheme structure of the simulated dual photoelectrode can effectively separate electrons and holes for simultaneous degradation of pollutants and hydrogen production to achieve the effective utilization of electrons of pollutants oxidation in the wastewater under the light and without additional power supply and accordingly hydrogen production efficiency was also significantly greater than MFC<sup>35-37</sup>. As is known to us, this construction of heterostructures can effectively facilitate the charge separation and transfer, shorter radial transfer path, and effectively reduce the charge recombination. Highly efficient photocatalytic H<sub>2</sub> generation under visible-light-driven was investigated based on MoS<sub>2</sub>/CdS nanosheets-on-nanorod and MoS<sub>2</sub>/CdS nanodots-on-nanorods, which exhibit excellent H<sub>2</sub> evolution rate and apparent quantum yield<sup>38,39</sup>.

Though the excellent performance was achieved in PEC applications, the formed electrons and holes must be consumed immediately and require continuous illumination to ensure the photocatalytic reaction can be carried out throughout the reaction period. Therefore, the biggest limitation of the traditional photocatalysts is the need for continuous light energy input. But in reality, the photocatalytic efficiency is closely related to the solar intensity of the day, while the light is not always present, and the electrons cannot be stored. So we envisioned the simultaneous collection and storage of solar energy for using in the dark. If the excited photogenerated electrons can be stored under the light illumination, it can not only reduce the recombination of photogenerated carriers, but also can continue to release the stored electrons for hydrogen production in the dark to convert solar energy into chemical energy, to enhance the efficiency of solar energy conversion, and further expand the application of solar energy in a certain extent.

Recently, the applicability of solar energy is extended to the dark stage by integrating the light harvesting and the energy storage system. A self-photorechargeability of WO<sub>3</sub> film was fabricated under visible light irradiation<sup>40-43</sup>, which can store and release on-demand<sup>44</sup>. Photocatalysts with storage capacity such as WO<sub>3</sub> or MoO<sub>3</sub> have been developed, and photoelectrons of TiO<sub>2</sub> can be transferred and stored in the conduction band of WO<sub>3</sub> or MoO<sub>3</sub> under UV irradiation and then the stored electrons are released from

WO<sub>3</sub> or MoO<sub>3</sub> for specific reactions in the dark<sup>45</sup>. In most research work, TiO<sub>2</sub> and WO<sub>3</sub> were combined into a composite photoelectrode<sup>41, 46-49</sup>. The electrons in the TiO<sub>2</sub> conduction band were implanted and stored in the WO<sub>3</sub> framework under UV irradiation, and then the stored electrons were released from WO<sub>3</sub> to reduce oxygen to H<sub>2</sub>O<sub>2</sub> and H<sub>2</sub>O in the dark. Similar charge storage phenomena have been reported in the dye-sensitized TiO<sub>2</sub>-WO<sub>3</sub> system. Upon illumination, excited electrons in the dye are injected into TiO<sub>2</sub> and WO<sub>3</sub> for electron storage. A solar rechargeable battery (solar water battery) was reported based on photoelectrochemical water oxidation, which is environmentally friendly and can provide an alternative to conventional photoelectrochemical water splitting<sup>50</sup>. The TiO<sub>2</sub> as photoelectrode was excited and generated electron-hole pair. Then the photogenerated electrons in the TiO<sub>2</sub>-PE were transferred to the WO<sub>3</sub>-SE through an external circuit and stored in situ and then release electrons to the Pt-CE for the reduction of hydrogen production in the dark. Dye-TiO<sub>2</sub>/electrolyte/Ni/WO<sub>3</sub> dye-sensitized solar rechargeable batteries were constructed by sol-gel method, which possessed higher energy density than similar materials<sup>51</sup>.

Therefore, in our work, a solar-charged photoelectrochemical cell (scPEWFC) was constructed for the phenol oxidization and hydrogen production and simultaneous electrons storage, which performed in a single chamber photoelectrochemical cell quartz reactor. Visible light response WO<sub>3</sub> NFs, C-Cu<sub>2</sub>O NWAs as photoanode and photocathode, respectively. The potential of the WO<sub>3</sub> NFs photoanode was higher than that of the C/Cu<sub>2</sub>O NWAs photocathode, resulting in the potential difference to spontaneously drive the photogenerated electrons of the WO<sub>3</sub> NFs photoanode to C/Cu<sub>2</sub>O NWAs photocathode from the external circuit to combine with the holes at the photocathode under the light, the holes of photoanode and electrons of photocathode thus can be released for organics degradation and water reduction. At the same time, the remaining photogenerated electrons were stored in the framework of WO<sub>3</sub> NFs structure for continuous discharge and hydrogen production throughout the day.

## Experimental Section

### 2.1. Materials

The tungsten foil (99.95%, 0.05 mm thick) and copper mesh (100 mesh, 0.11 mm dia wire) were purchased from Alfa Aesar (China) Chemical Co., Ltd. Sulphuric acid (AR, 98%), sodium hydroxide (AR, 99%), sodium fluoride (AR, 99%), sodium sulfate (AR, 98%), ethanol (AR, 99.5%), acetone (AR, 99.5%) and isopropanol (AR, 99%) were purchased from Sinopharm Chemical Reagents Co., Ltd., SCRC, China. Phenol (D6, 98%) was purchased from CIL Cambridge isotope laboratories Inc.

### 2.2 Preparation of WO<sub>3</sub> NFs Photoelectrode

WO<sub>3</sub> NFs photoanode was prepared by anodizing according to the literature<sup>44</sup>. The tungsten foil (Alfa Aesar, 99.95%, 0.05 mm thick) was cut into 1.5 x 5.0 cm pieces and then polished to a mirror with 180 Cw, 300 Cw, 600 Cw and metallographic sandpaper to remove rust and oxide on the surface, rinsed with distilled water, and ultrasonically cleaned in distilled water, acetone, ethanol, isopropanol and distilled water for 10 min, respectively. The anodizing device is composed of two electrode systems with a

platinum foil as the counter electrode (cathode) and the tungsten foil as the working electrode (anode); the distance was kept constantly at 2 cm between the cathode and the anode. The tungsten foil was anodized at a constant potential (+50 V) using a DC power supply (Sovotek, E5200-3 75v/2A DC Power Supply, Da Hua Electronic, China) for 70 min (50 min, 60 min, 80 min, 90 min) under controlled magnetic stirring at a temperature of 15 °C and the electrolyte solution containing 1 mol L<sup>-1</sup> H<sub>2</sub>SO<sub>4</sub> and 0.5 wt.% NaF. After the anodization process, the samples were soaked in distilled water and ethanol for 30 min, then rinsed with distilled water, and dried in air. Hereafter the WO<sub>3</sub> films were calcined at 400 °C for 4 h in air atmosphere, the rate of heating was maintained at 2 °C min<sup>-1</sup> and naturally cooled to room temperature.

### 2.3. Preparation of C/Cu<sub>2</sub>O NWAs Photoelectrode

Copper mesh (Alfa Aesar, 100 mesh, 0.11 mm dia wire) was cut into pieces about 1.5 cm×5 cm and sonicated in acetone, deoxygenated deionized water and absolute ethanol for 15 min and dried in air. The Cu(OH)<sub>2</sub>NWs were prepared by the constant current anodic method in a conventional three electrodes system using CHI 660C electrochemical workstation (CH Instruments Inc., USA) with the electrolytes solution containing 3 mol L<sup>-1</sup> sodium hydroxide solution at room temperature<sup>52</sup>. Ag/AgCl was used as the reference electrode, Pt as the counter electrode and the copper mesh as the working electrode. Cu(OH)<sub>2</sub> NWs were produced by anodizing at a constant current of 10 mA cm<sup>-2</sup> for 30 min, and the electrode potential is stabilized at -0.24 V (vs Ag/AgCl) at the initial stage. When the potential was changed suddenly, it can be considered anodizing has been completed. The prepared Cu(OH)<sub>2</sub>NWs were rinsed with deionized water, dried in vacuum and then immersed in a glucose solution at a concentration of 3 g L<sup>-1</sup> for 1 min, then taken out and dried at room temperature. The glucose-loaded Cu(OH)<sub>2</sub> NWs were calcined at 550 °C for 4 h in N<sub>2</sub> atmosphere, the rate of heating was maintained at 4 °C min<sup>-1</sup>, finally at a rate of 5 °C min<sup>-1</sup> decreased to room temperature to obtain the C/Cu<sub>2</sub>O NWAs photocathode.

### 2.4. Materials characterization

The detailed morphology and microstructure feature of the samples were observed by field emission scanning electron microscopy (FE-SEM, Hitachi S-4800, Japan) and high resolution transmission electron microscopy (HR-TEM, JEM2100, JEOL, Japan, using a JEM-2000EX electron microscope operated at 200 kV). The composition and structure of the samples were characterized via X-ray diffraction (XRD, D8 Focus X-ray diffractometer, Bruker, Germany), using a Cu target:  $\lambda = 1.540598 \text{ \AA}$ ; tube voltage 40 kV; tube current 60 mA; scanning speed 2° min<sup>-1</sup>. The composition, structure and bonding conditions of the samples were characterized and tested by Raman (514 nm laser with RM100). UV-Vis diffuse reflectance spectroscopy (UV-Vis DRS, Avantes, Netherlands) was used to determine the optical absorption properties of the sample electrodes.

### 2.5. Photoelectrochemical measurements

The photoelectrochemical properties of these sample electrodes were tested on a CHI660C electrochemical station (CH Instruments Inc., USA) by using a conventional three-electrode system at room temperature. Sample electrode, Pt, Ag/AgCl electrode as the working electrode, counter electrode and the reference electrode, respectively. PEC is achieved using a two-electrode device. A 300W high voltage Xe lamp (Changtuo,

China) was used as a simulated solar light source (wavelength range of 420-800 nm, light intensity of 100 mW cm<sup>-2</sup>) in a single chamber photoelectrochemical quartz reactor. No further description, all experiments are carried out under the AM1.5 filter. Photoanode and photocathode working area are 2 cm<sup>2</sup>, moderate agitation and no external voltage. Before the test, it is necessary to continuously pass nitrogen into the electrolyte for 30 min to remove other impurities such as dissolved oxygen in the solution. The I-V characteristic curve was measured by linear sweep voltammetry (LSV) with a sweep speed of 0.02 V s<sup>-1</sup>. The power density (P) is calculated as follows:  $P = I \times V$ . Under the irradiation of AM 1.5, the degradation of the organic compound was carried out in a quartz reactor. Phenol (20 mg L<sup>-1</sup>) as the target organic compound with the electrolytes solution containing 0.1 mol L<sup>-1</sup> Na<sub>2</sub>SO<sub>4</sub>. The removal rate of phenol total organic carbon was monitored by the N/C3100 TOC/TN analyzer (Analytikjena, Germany). The total hydrogen amount produced was calculated by multiplying the hydrogen content in a 1 mL gas sample by the headspace volume of the PEC reactor (200 mL). Hydrogen is qualitatively measured by gas chromatography (GC 7900, Techcomp, Shanghai, China), N<sub>2</sub> as carrier gas, TCD detector, column temperature of 80 °C, detector temperature of 150 °C, Inlet port temperature of 130 °C and sample volume of 1 mL. Gas chromatography-mass spectrometry (GC-MS, Agilent 6890/5973 N, Agilent Co) were utilized to detect the D<sub>2</sub>, DH and H<sub>2</sub>.

## Results and discussion

### 3.1. Anode oxidation for phenol efficient conversion

As shown in Fig. 1A, the TOC removal rate of phenol of WO<sub>3</sub> NFs- C/Cu<sub>2</sub>O NWAs was 82.12% in the first 8 h under AM 1.5 illumination, which is higher than that of WO<sub>3</sub> NFs-Pt (TOC removal rate 52.5%). The reason for this efficient oxidation is similar to that reported in the literature. Under such conditions, a simulated Z-Scheme type dual photoelectrode solar-charged photoelectrochemical wastewater fuel cell (scPEWFC) was constructed. Due to the presence of the Fermi level difference, the photogenerated electrons of the photoanode were migrate to the photocathode to combine the holes at the photocathode, so that the photogenerated electrons and holes were difficult to recombine, so the catalytic oxidation efficiency of phenol has been greatly improved. After the illumination for 8 h, the whole system were kept in the dark for 8 h. The TOC removal of phenol have not changed whether the photoanode and photocathode were disconnected or not. It is speculated that in the absence of light source, without holes were produced in the anode, the entire anode filed lacks the oxide species, so the phenol won't be further removed under the drak.

In Fig. 1C, it's also show that the photocurrent of the single WO<sub>3</sub> NFs photocathode is very small, but the photocurrent density of C/Cu<sub>2</sub>O NWAs can reach 0.37 mA cm<sup>-2</sup>, and the short circuit current (J<sub>SC</sub>) of scPEWFC is 0.42 mA cm<sup>-2</sup>, which is greater than the sum of the two, and these values are also larger than the literature<sup>34</sup>. So it can be inferred that the cathode and anode of the constructed scPEWFC have a synergistic effect, which confirm that the cell performance of WO<sub>3</sub> NFs-

ARTICLE

Journal Name

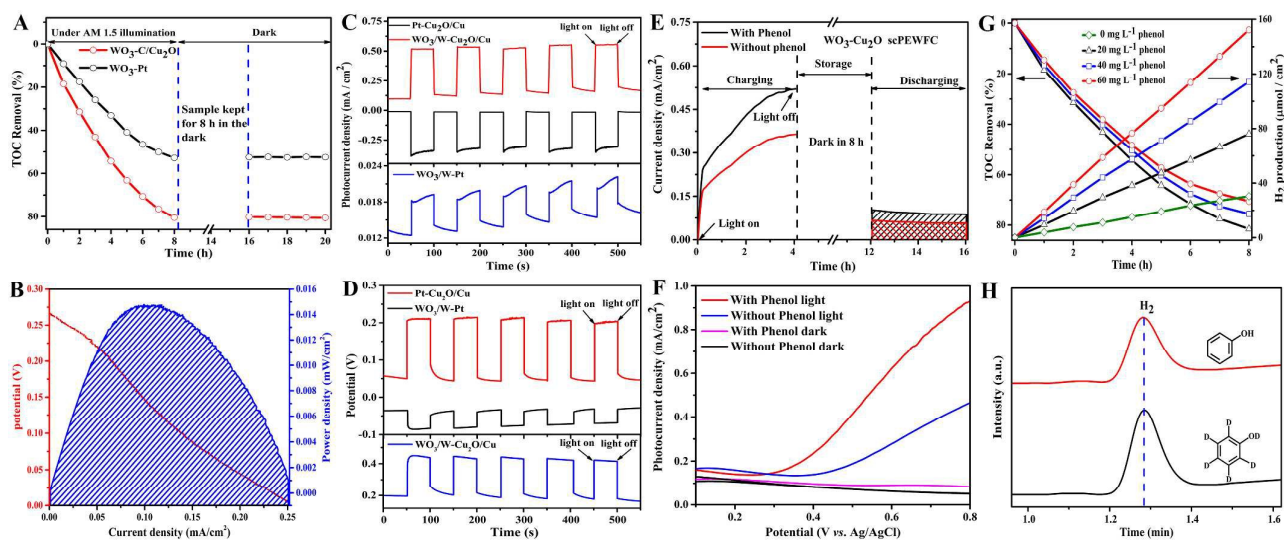


**Fig. 1** The TOC removal rate (A) of phenol ( $20 \text{ mg L}^{-1}$ ) for scPEWFC under light illumination and dark. The I–V characteristic curve (B) (red) and power density curve (blue) of  $\text{WO}_3$  NFs-C/ $\text{Cu}_2\text{O}$  NWAs scPEWFC. The I–V curves were performed by linear sweep voltammetry with a two electrode system in one typical cycle. The scan rate was  $0.05 \text{ V s}^{-1}$ . The photocurrent density (C) and the open-circuit voltage (D) of  $\text{WO}_3$  photoanode and C/ $\text{Cu}_2\text{O}$  photocathode were measured in the dark and under AM1.5 ( $100 \text{ mW cm}^{-2}$ ) illumination. The I–t characteristics curves (E), LSV (F) were recorded with no external bias from the scPEWFC using two electrode configuration under AM1.5 illumination in the  $0.1 \text{ mol L}^{-1} \text{ Na}_2\text{SO}_4$  solution containing  $20 \text{ mg L}^{-1}$  phenol (the red solid line) and without phenol (the black solid line). The amount of hydrogen production and TOC removal rate (G) were recorded in the  $0.1 \text{ mol L}^{-1} \text{ Na}_2\text{SO}_4$  solution containing different concentration phenol. The deuterium-labelling phenol (D6,  $20 \text{ mg L}^{-1}$ ) and non-labelling phenol (H) were performed to prove the source of hydrogen.

C/ $\text{Cu}_2\text{O}$  NWAs is superior<sup>53,54</sup>. In such a simulated Z-Scheme system, the electron/hole pairs were separated effectively at the two photoelectrodes. The holes of  $\text{WO}_3$  NFs photoanode and the electrons of C/ $\text{Cu}_2\text{O}$  NWAs photocathode can be released for the oxidation of the phenol and the reduction of proton to produce hydrogen, respectively. In addition, after five cycle tests of dark and light, the photocurrent density almost keeps stable, which indicated that the  $\text{WO}_3$  NFs photoanode has a good photoelectrochemical response, photocurrent stability, anti-corrosive properties. However, when Pt foil as cathode, the photocurrent is relatively low, due to without Z-scheme cell was constructed. At the same time, the photovoltage was also measured. As shown in Fig. 1D, the photovoltage of  $\text{WO}_3$  NFs photoanode is almost low, and exhibit a relatively slow photoresponse. But the C/ $\text{Cu}_2\text{O}$  NWAs photocathode display excellent photoresponse (photovoltage increases instantly to  $0.15 \text{ V}$  and keeps stable). The open-circuit voltage ( $V_{\text{OC}}$ ) of  $\text{WO}_3$  NFs-C/ $\text{Cu}_2\text{O}$  NWAs scPEWFC is  $0.26 \text{ V}$ . In other words,  $\text{WO}_3$  NFs photoanode provide a negative bias for C/ $\text{Cu}_2\text{O}$  NWAs photocathode, while C/ $\text{Cu}_2\text{O}$  NWAs photocathode offered a positive bias for  $\text{WO}_3$  NFs photoanode. Because the  $\text{WO}_3$  NFs photoanode Fermi level is more negative than that of C/ $\text{Cu}_2\text{O}$  NWAs photocathode, an interior bias can be produced to drive the electrons of  $\text{WO}_3$  NFs to C/ $\text{Cu}_2\text{O}$  NWAs electrode without the external conditions.

The Mott-Schottky curve of  $\text{WO}_3$  NFs photoelectrode is shown in Fig. S1 (ESI<sup>†</sup>), which illustrate the relationship between  $1/C^2$  and the applied potential.  $\text{WO}_3$  NFs electrode is characterized by a positive slope in the Mott-Schottky plot, which means the sample is an n-type semiconductor material. The tangent portion of the curve intersects with  $1/C^2=0$  is the flat potential  $E_{\text{FB}}$  of the  $\text{WO}_3$  NFs photoelectrode and it can be

estimated that the  $E_{\text{FB}}$  of  $\text{WO}_3$  NFs is  $0.30 \text{ V}$  (vs. Ag/AgCl) in  $\text{Na}_2\text{SO}_4$  solution. Meanwhile,  $\text{WO}_3$  NFs electrode photocarrier density can be calculated and presented ND values of  $4.47 \times 10^{20} \text{ cm}^{-3}$ . Compared with other materials,  $\text{WO}_3$  NFs have a higher carrier concentration<sup>55</sup>. The results show that  $\text{WO}_3$  NFs photoelectrode has a very high photocatalytic oxidation ability, excellent photoresponse and rapid charge transfer rate.

### 3.2 Cathode reduction for sustainable hydrogen production

In the system, oxidation of phenol was performed at the anode, meanwhile efficient hydrogen production was operated at the cathode. Many literatures were reported that the hydrogen production efficiency of the cathode is limited by anodic oxidation<sup>54,56,57</sup>, in other words, the whole system, the oxidation of anode phenol is the rate-limiting step.

From the thermodynamic point of view, the oxidation potential of lots of organic pollutants is lower than that of water. Therefore, phenol was selected as a representative organic pollutant to study the degradation performance of the scPEWFC. In fact we are also very interested in studying the effect of different pollutants oxidation on the hydrogen production of the cathode, and the relevant work was also carried out. In the previous work, two classes of typical pollutants, phenols and alkylbenzenes, were treated using a self-biasing photoelectrochemical (PEC) cell to reveal the intrinsic relationships between the redox properties of the pollutants and hydrogen production<sup>58</sup>. The photocatalytic oxidation of phenol and simultaneous hydrogen production were studied by using phenol as the oxidizing substrate and  $\text{WO}_3$  NFs electrode as the photoanode and C/ $\text{Cu}_2\text{O}$  NWAs as the photocathode.

The photocatalytic oxidation of phenol and simultaneous hydrogen production were studied by using phenol as the

oxidizing substrate and WO<sub>3</sub> NFs electrode as the photoanode and C/Cu<sub>2</sub>O NWAs as the photocathode. The i-t curve was determined in the two-electrode system in 0.1 mol L<sup>-1</sup> Na<sub>2</sub>SO<sub>4</sub> solution containing 20 mg L<sup>-1</sup> phenol under the AM1.5 filter irradiation (100 mW cm<sup>-2</sup>), without an external bias as shown in Fig. 1E. With the prolongation of illumination time, the photocurrent density tends to increase gradually. In the initial absence of light, the photocurrent density was almost zero, and then applied the light, the photocurrent density increases slowly with the time, then gradually stabilized and remained at 0.523 mA cm<sup>-2</sup> after 4 h operation. For comparison, without phenol was added into the 0.1 mol L<sup>-1</sup> Na<sub>2</sub>SO<sub>4</sub> electrolyte solution. Correspondingly, the photocurrent density was significantly lower than the presence of phenol. After keeping in dark for 8 h, the photocurrent was measured again, a similar result occurs. In the test of hydrogen production, it was notable that the amount of hydrogen production was about 30.74 μmol cm<sup>-2</sup> in the absence of phenol. In contrast, in the presence of phenol (20 mg L<sup>-1</sup>), the amount of hydrogen production reached 79.58 μmol cm<sup>-2</sup> as shown in Fig. 1G. Some literatures also reported that the nature of the pollutions as well as its concentration also had great influence on the performance for PEC hydrogen production from the biomass derivative and water<sup>57</sup>. With the increase of pollutant concentration, the hydrogen production effect was obviously enhanced. This also illustrates that the oxidation of phenol at the anode did play a decisive role in the hydrogen production of the cathode, the electrons of the anodic oxidation transferred to the cathode to raise the photocurrent density, and accordingly enhance the efficiency of hydrogen production. Therefore, the oxidation reaction of the anode was easier to proceed, and the efficiency of hydrogen production was more obvious.

In order to understand the effect of phenol and optimize scPEWFC activity for phenol oxidation over the WO<sub>3</sub> NFs photoanode, the linear sweep voltammetry (LSV) plots of the as-prepared photoanode was performed in 0.1 mol L<sup>-1</sup> Na<sub>2</sub>SO<sub>4</sub> solution containing 20 mg L<sup>-1</sup> phenol whether with illumination or not. As shown in Fig. 1F, the WO<sub>3</sub> NFs showed higher current density in the phenol solution (0.09 mA cm<sup>-2</sup>) than that of without phenol (0.04 mA cm<sup>-2</sup>) under dark at 0.8 V (vs. Ag/AgCl). When the surface of the electrode was irradiated with simulated sunlight, the current density of the WO<sub>3</sub> NFs photoelectrode was significantly increased to 0.92 mA cm<sup>-2</sup> at 0.8 V (vs. Ag/AgCl). The results indicated that phenol was more easily oxidized under simulated solar excitation, and the oxidation potential was 0.35 V (vs. Ag/AgCl) (lower than water oxidation), which explained the reason of phenol oxidation at the anode to promote cathode hydrogen production at the cathode.

In addition, it is possible that hydrogen can be derived from the splitting of water or degradation of phenol, so a comparative experiment is carried out by using deuterium-labeled phenol (D6, 20 mg L<sup>-1</sup>) to prove the source of hydrogen. By GC-MS analysis, only H<sub>2</sub> is detected and no DH or D<sub>2</sub> is detected during the photoelectrocatalysis experiment (as shown in Fig. 1H), so it can be illustrated that hydrogen is derived from the water splitting.

### 3.3 The relationship between electrons storage of WO<sub>3</sub> and hydrogen production

In the Fig 1E, when the cathode and anode were disconnected and remained in the dark for 8 h, and then connected the cathode and the anode again, and it was apparent that the photocurrent was observed significantly, and higher than the initial dark current. WO<sub>3</sub> NFs photocharging characteristics are reported in many literatures, so it was can be speculate that part of the excited electrons were stored within the WO<sub>3</sub> NFs electrode in the system (the shaded area below the discharge curve corresponds to the total stored charges) and were discharged in the dark. Therefore, it was concluded that when the WO<sub>3</sub> NFs as scPEWFC anode material, the characteristics of light-charging was still remained and the mechanism is explained as follows:

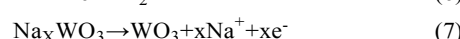
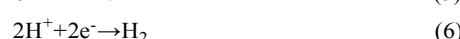
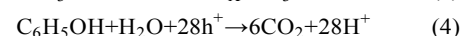
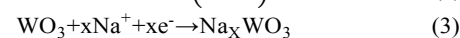
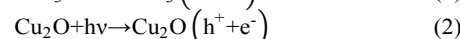
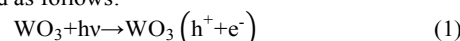
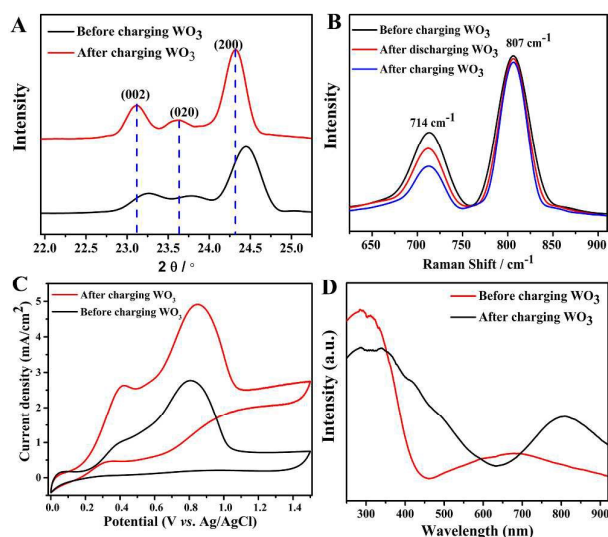


Fig. S2 (ESI†) describes the schematic plots of photocharging and discharging processes of WO<sub>3</sub> NFs during light and dark conditions. The photogenerated electron-hole pairs were formed under simulative solar light illumination. When the WO<sub>3</sub> NFs were excited (Eqn 1) the part of the photo-excited electrons can be neutralized by the intercalation of existing Na<sup>+</sup> in the electrolyte solution in the form of Na<sub>x</sub>WO<sub>3</sub>, which stored within the WO<sub>3</sub> framework in situ (Eqn 3). The phenol molecules adsorbed on the electrode surface were oxidized to CO<sub>2</sub> by the holes generated on the WO<sub>3</sub> electrode (Eqn 4). The carbon-coated C/Cu<sub>2</sub>O NWAs/Cu mesh also generated electron-hole pairs under the simulative solar light illumination (Eqn 2). The n-type semiconductor WO<sub>3</sub> NFs (E<sub>g</sub>=2.75 eV), p-type semiconductor C/Cu<sub>2</sub>O NWAs (E<sub>g</sub>=2.4 eV), and the relative band positions for the WO<sub>3</sub> NFs-C/Cu<sub>2</sub>O NWAs visible-light response dual-photoelectrodes as shown in Fig. S3 (ESI†). According to the principle of energy level matching, the Fermi level of the n-type semiconductor WO<sub>3</sub> NFs was higher than that of the p-type semiconductor C/Cu<sub>2</sub>O NWAs, Accordingly, the potential of the WO<sub>3</sub> NFs photoanode was higher than that of the C/Cu<sub>2</sub>O NWAs photocathode under AM 1.5 illumination, and the interior bias was generated and to drive the electrons of WO<sub>3</sub> NFs photoanode to combine with the holes of C/Cu<sub>2</sub>O NWAs photocathode from the external circuit (Eqn 5). The holes of WO<sub>3</sub> NFs photoanode and the electrons of C/Cu<sub>2</sub>O NWAs photocathode can be released for the oxidation of the phenol at the anode and the reduction of proton to produce hydrogen at the cathode (Eqn 6,8). Afterwards, Na<sup>+</sup> de-intercalate from the WO<sub>3</sub> NFs structure (Eqn 7), then stored electrons were released and transferred to C/Cu<sub>2</sub>O NWAs counter electrode to produce hydrogen (Eqn 8).

Meanwhile, the structure of Z-scheme is more favorable for the separation of photogenerated electrons and holes, and enhance the efficiency of photoelectrocatalysis conversion.

In order to prove that  $\text{Na}^+$  was embedded into the framework of  $\text{WO}_3$  NFs under AM 1.5 illumination. XRD was used to characterize the variety of  $\text{WO}_3$  NFs framework before and after charging and discharging process in  $0.1 \text{ mol L}^{-1} \text{ Na}_2\text{SO}_4$  electrolyte solution containing  $20 \text{ mg L}^{-1}$  phenol as shown in Fig. 2A. The three peaks of  $2\theta=23.119^\circ$ ,  $23.586^\circ$  and  $24.380^\circ$  corresponding to the (002), (020) and (200) planes are characteristic peaks of the monoclinic phase  $\text{WO}_3$ . After performing three charge-discharge cycle, the characteristic peaks shift to a lower  $2\theta$  value, which is associated with the structural change of tetragonal structure and which is related to the embedding of the alkaline cations as discussed in the literature<sup>59, 60</sup>. Thus, the results further demonstrate that the presence of trapped alkali cations in the framework of  $\text{WO}_3$  NFs in situ. Raman spectroscopy was also used to study the structural variety in higher symmetry caused by intercalation of the alkaline cations. Fig. 2B shows the Raman spectra of the  $\text{WO}_3$  NFs photoelectrode after the three charge-discharge cycle in the  $\text{Na}_2\text{SO}_4$  electrolyte containing  $20 \text{ mg L}^{-1}$  phenol. The Raman shift peak at  $807 \text{ cm}^{-1}$  and  $714 \text{ cm}^{-1}$  are attributed to the stretching modes arising from the W-O framework in monoclinic  $\text{WO}_3$ <sup>61, 62</sup>. It is possible to determine initially that the electrode was monoclinic phase  $\gamma\text{-WO}_3$ . The peak at  $807 \text{ cm}^{-1}$  is hardly altered by the phase transition, while the mode at  $714 \text{ cm}^{-1}$  is highly sensitive to the embedded ions, which reflects the structural changes caused by the embedded ions. When the  $\text{WO}_3$  NFs were irradiated for 8 h, the peak intensity at  $714 \text{ cm}^{-1}$  decreased which is associated with the changes in the  $\text{WO}_3$  host [to a more symmetrical structure (tetragonal)] and ascribed to the symmetrisation of W-O bonds along the a-b plane of the  $\text{WO}_6$  octahedron<sup>59, 63, 64</sup>. When the  $\text{WO}_3$  NFs were discharged for 4 h, the intensity of the peak at  $714 \text{ cm}^{-1}$  restores to the original state. Therefore, the greater the decrease in the Raman intensity of the  $714 \text{ cm}^{-1}$  peak, the more trapped alkali cations stored within the  $\text{WO}_3$  structure, and the more electrons stored.



**Fig. 2** XRD patterns (A), Raman patterns (B), Cyclic voltammetry curve (C) and UV-Vis absorption spectra (D) of  $\text{WO}_3$  NFs before and after three charge-discharge cycles performed in  $0.1 \text{ mol L}^{-1} \text{ Na}_2\text{SO}_4$  electrolyte solution containing  $20 \text{ mg L}^{-1}$  phenol.

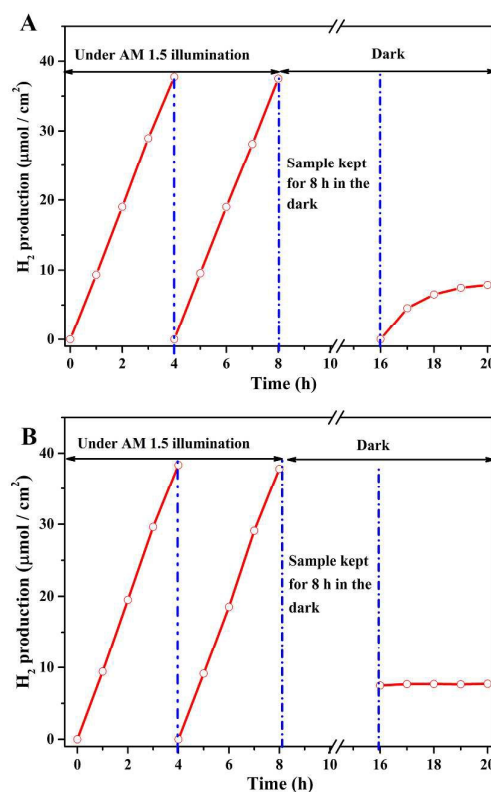


**Fig. 3** Amount of hydrogen produced under different conditions. The cathode and anode were disconnected (A) or connected (B) for 8 h under the dark.

The mechanism of scPEWFC photo-charging and discharging ( $\text{Na}^+$  intercalation and deintercalation from the  $\text{WO}_3$  framework) was studied by using cyclic voltammetry. Fig. 2C depicts the CV response of  $\text{WO}_3$  before and after 10 min illumination. A significant oxidized peak ( $0.40 \text{ V vs. Ag/AgCl}$ ) was presented under the visible irradiation for 10 min, which was attributed to the phenol oxidation at the photoanode. The presence of other anode peaks ( $0.82 \text{ V vs. Ag/AgCl}$ ) may be caused by the localised oxidation of  $\text{W}^{4+}$  to  $\text{W}^{5+}$  or  $\text{W}^{5+}$  to  $\text{W}^{6+}$ , and was related to the photo-charging phenomenon, which reflected the discharging of stored electrons and simultaneous de-intercalation of alkali cations<sup>65</sup>. Fig. 2D is UV-visible diffuse reflectance absorption spectra of the  $\text{WO}_3$  NFs photoelectrode. It shows that the prepared  $\text{WO}_3$  NFs photoelectrode. It shows that the prepared  $\text{WO}_3$  NFs absorption band edge can reach about  $450 \text{ nm}$ , barely enter the visible light response range. The bandgap of  $2.75 \text{ eV}$  was calculated according to the formula, which is the same as reported in the literature<sup>66</sup>. While, the absorption band is clearly redshift to  $550 \text{ nm}$  and the absorption band of visible light section is present, which speculates that  $\text{Na}^+$  in the electrolyte solution were intercalated into the  $\text{WO}_3$  structure in situ in the form of tungsten bronze.

In addition, it can be speculated that the  $\text{Na}^+$  has been successfully embedded into the structural framework of  $\text{WO}_3$  after 10 min light from the EDS energy spectrum (as shown in Fig. 4H), which can explain the charge-discharge

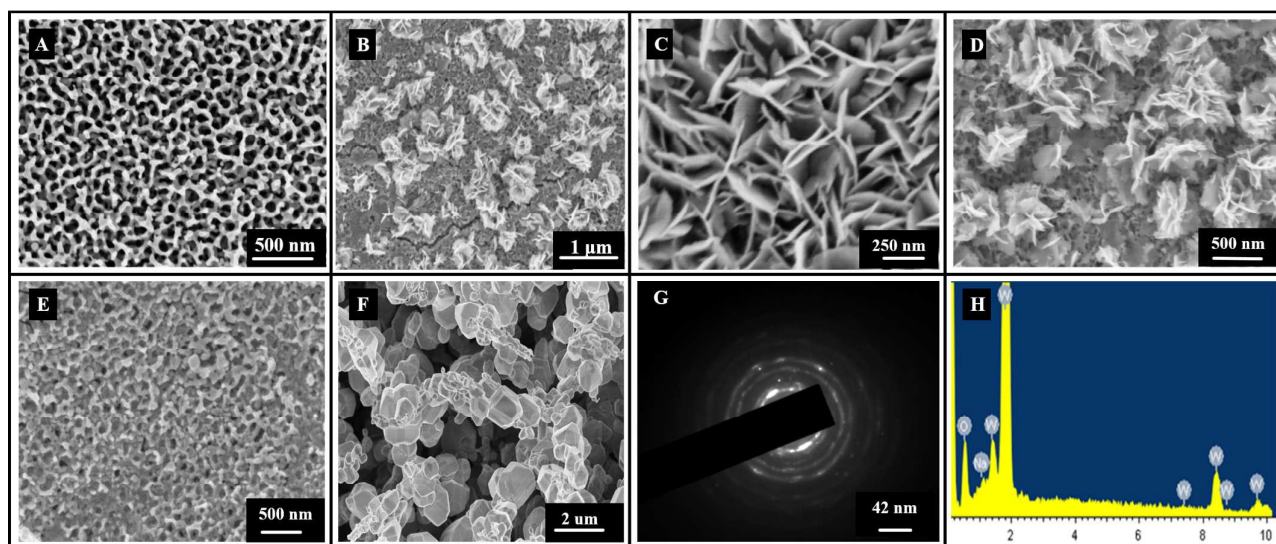


**Fig. 4** (A), (B), (C), (D) and (E) are the SEM image of  $\text{WO}_3$  NFs at the time of anodized 50, 60, 70, 80 and 90 min, respectively. (F) and (G) are the SEM and SAD spectrum of  $\text{C}/\text{Cu}_2\text{O}$  NWAs. (H) is EDS elemental analysis of  $\text{WO}_3$  NFs after 10 min charging.

principle of the  $\text{WO}_3$  NFs electrode to a certain extent.

When the charges is being stored at the anode, hydrogen is also being produced at the cathode simultaneously. The research method of hydrogen production process is the same as the TOC removal. The amount of hydrogen production was  $79.58 \mu\text{mol cm}^{-2}$  and showed a significant linear increase for 8 h under the AM 1.5 illumination. The anode and cathode were disconnected and kept in the dark for 8 h, and then connected the cathode and the anode again, the hydrogen production increased to  $12.5 \mu\text{mol cm}^{-2}$  for 4 h gradually as shown in Fig. 3A. In contrast, the dark process was not disconnected for 8 h, it can show that the amount of hydrogen were maintained at about  $10 \mu\text{mol cm}^{-2}$  for 4 h without any change as shown in Fig. 3B. Considering the variety of TOC, it can speculate the main reason is that, the photoelectrons of  $\text{WO}_3$  NFs photocathode were separated from the holes after the illumination, and some of the photoelectrons of  $\text{WO}_3$  NFs photoanode were driven to combine with the holes of  $\text{C}/\text{Cu}_2\text{O}$  NWAs photocathode from the external circuit to increase the utilization of cathode photogenerated electrons. The other part of the photoelectrons was stored in the lattice of the anode  $\text{WO}_3$  NFs in situ. If the anode and cathode were not connected in the dark for 8 h, then the electrons stored in the  $\text{WO}_3$  NFs will be transferred to the cathode for hydrogen production in situ, which has been stored in the reactor all the time, so the amount of hydrogen remained stable essentially when it was detected. On the contrary, if the dark process was disconnected for 8 h, it can be seen that the amount of hydrogen production increased gradually after connecting the two electrode. During the process of disconnection, the electrons at the anode have been stored without discharging, then the electrons stored on the anode will be transferred to the cathode through the external circuit after the reconnection, so that the stored electrons can continue be utilized for hydrogen production under dark conditions. Therefore, it can be concluded that the photoelectrons can be introduced into the cathode to combine with the holes on the

$\text{C}/\text{Cu}_2\text{O}$  NWAs; meanwhile, the photoelectrons were stored in situ to achieve the purpose of hydrogen production throughout the day even in the absence of light, and the utilization rate of stored electrons was 98.23%.

Thus, it can found that the construction of cPEWFC can not only efficient oxidation of phenol, store the electrons, but also obtain hydrogen, with great significance of environmental and energy. The part of the photoelectrons generated by  $\text{WO}_3$  under photoexcitation was stabilized by the alkaline cations and stored within the  $\text{WO}_3$  framework in situ, and this charges of light-induced storages were utilized subsequently under dark conditions in a controllable manner. Therefore, the factors that affect the directional movement of alkaline cations can affect the  $\text{WO}_3$  NFs charging and discharging capacity, such as the type of alkaline cation, the size, the concentration of electrolyte, the surface resistance of semiconductor  $\text{WO}_3$  NFs photoanode. The properties of the interface between the scPEWFC electrode and the electrolyte solution by using the electrochemical impedance spectroscopy (EIS) were investigated. First, the morphological structure of  $\text{WO}_3$  were studied by adjusting the anodizing time (50 min, 60 min, 70 min, 80 min, 90 min) to obtain the different structure of  $\text{WO}_3$ .

Fig. S4 (ESI†) is the Nyquist curve of  $\text{WO}_3$  photocathode prepared at different anodizing times. As it can be seen from the Fig. S4 (ESI†),  $\text{WO}_3$  photoanode exhibits the minimum diameter of the semicircle under the condition of 70 min, which indicated the optimal conductivity and fast electron transfer process occurring at its surface. This can also be speculated from its appearance as shown in Fig. 4. When the anodizing time was 50 min (Fig. 4A),  $\text{WO}_3$  was mainly composed of broken nanotube network structure, and the pore structure was very obvious, but the nanotube fracture was severe, so its impedance increased evidently. When the anodizing time increased (60 min Fig. 4B), the morphology of the nanoflower was gradually displayed. Under the anodic conditions of 70 min (Fig. 4C), a dense nanostructure was formed, the surface was

uniform and the resistance became smaller. The reason for this is that the nanotube had a high specific surface area that can generate more photogenerated carriers and adsorb more contaminants on the surface. At the same time, the petal structure was also more conducive to the absorption and utilization of light energy. Whereas, with the extension of the anodizing time (80 min Fig. 4D), the nanoflower structure became scarce. The possible reason is that the anodizing time was too long, and the existing nanoflowers were further etched, the lower part of the pipe network has been blocked. After increasing the anodizing time to 90 min (Fig. 4E), the nanostructure disappeared completely, while the underlying pipe network structure completely blocked, resulting in its increasing impedance. Fig. 4(F) and (G) are the SEM and TEM image of C/Cu<sub>2</sub>O NWAs, respectively. The diameter of C/Cu<sub>2</sub>O NWAs was about 500 nm, and smooth surfaces with no obvious fractures, the nanowires are densely grown on the Cu

mesh surface, which greatly increases the surface area of the electrodes. The performance tests of the scPEWFC were carried out by using a two-electrode system. The I-V characteristic curve was measured by linear sweep voltammetry with a sweep speed of 0.02 V s<sup>-1</sup>. The power density (P) is calculated as follows:  $P = I \times V$ .

In Fig. 1B, when the current density is 0.10 mA cm<sup>-2</sup>, the power density reaches a maximum (P<sub>max</sub>) of 0.015 mW cm<sup>-2</sup>. The fill factor (FF) which is also an important indicator of output characteristics of a photoelectrochemical cell can be calculated based on these parameters by the following equation:

$$FF = \frac{P_{\max}}{J_{\text{SC}} \cdot V_{\text{OC}}}$$

Where P<sub>max</sub> and J<sub>SC</sub>•V<sub>OC</sub> represent the actual maximum power density and the theoretical maximum power density, respectively. J<sub>SC</sub> is the short-circuit current density, V<sub>OC</sub> is the open-circuit voltage. Table S1 (ESI†) lists the battery properties of WO<sub>3</sub> NFs -C/Cu<sub>2</sub>O NWAs scPEWFC prepared at different anodizing times. These results also demonstrate that J<sub>SC</sub> exhibits a maximum value with the increase of anodic time. The removal of TOC and the amount of hydrogen production follow the same trend. The WO<sub>3</sub> electrode (anodized of 70 min) behave the best performance, which also be attributed to its surface microscopic structure.

The factors influencing the charge and discharge properties of WO<sub>3</sub> were also investigated. As can be seen from Table. S2 (ESI†), the electrolyte concentration is not the larger the charge and discharge performance is better. When the electrolyte concentration is 0.1 mol L<sup>-1</sup>, the optical photocurrent density reached to the maximum. It is also indicate that WO<sub>3</sub> stores more charges in 0.1 mol L<sup>-1</sup> Na<sub>2</sub>SO<sub>4</sub> electrolyte solution and the amount of hydrogen in the dark also reached the maximum. To some extent, the charge stored in WO<sub>3</sub> can be used efficiently for hydrogen production in the dark. It is speculated the main reason for this is that the size of the alkaline cations themselves are different, so the rate of intercalation and de-intercalation of Na<sup>+</sup> is different, so that the charge and discharge capacity is different. While the discharge speed will directly affect the dark current. Therefore, due to the different discharge speed, the demand for alkaline cations concentration is different, as for Na<sup>+</sup> itself, 0.1 mol L<sup>-1</sup> is the optical concentration.

It can be found that the degradation of pollutants and hydrogen production systems remained stable in the solar-charged photoelectrochemical wastewater fuel cell (scPEWFC) by performing three cycles testing of the hydrogen production and TOC removal (as shown in Fig. 5). The WO<sub>3</sub> electrode was illuminated under the simulative solar light for 4.2 h and then discharged in the dark for 4.2 h. After three cycles, the electrodes showed good stability and recyclability for all three cycles.

## Conclusions

In summary, a visible responsive dual photoelectrode based on WO<sub>3</sub> NFs-C/Cu<sub>2</sub>O NWAs scPEWFC was constructed for the simultaneous treatment of wastewater and hydrogen production. The scPEWFC

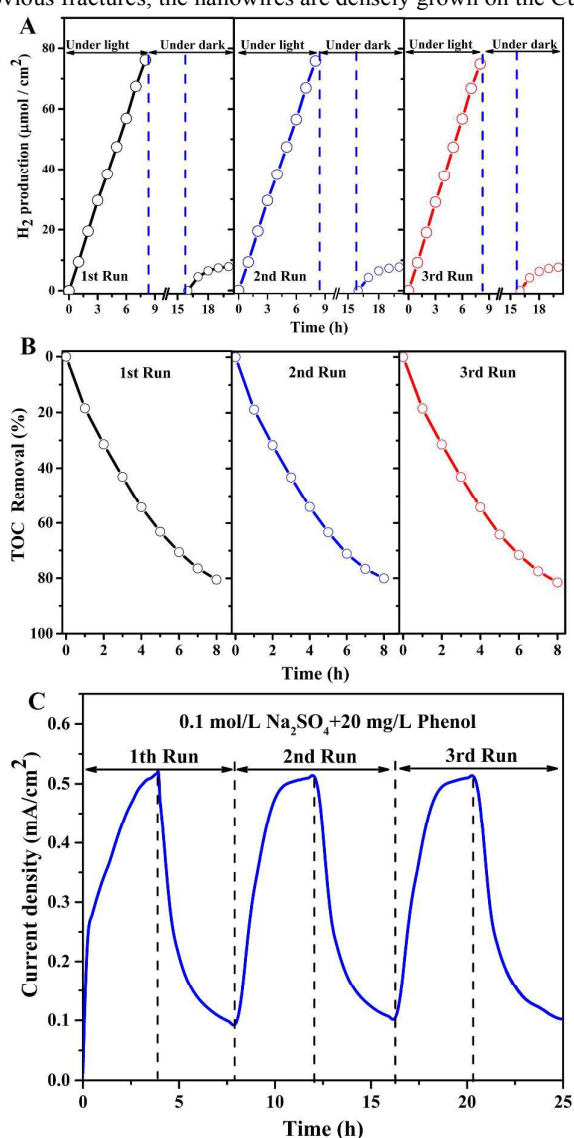


**Fig. 5** The stability of scPEWFC in hydrogen production (A), TOC removal (B), and three cycles of on-off visible light irradiation (C) were recorded.

performance parameters, the ability of deal with pollutants, hydrogen production and the mechanism of scPEWFC charging-discharging were systematically investigated. In the work, the hydrogen production of scPEWFC based on phenol oxidation is 3.02 times higher than that of pure photocatalytic water splitting, which indicated that the oxidation of phenol could effectively promote the hydrogen production. In addition, it also show that WO<sub>3</sub> NFs still retain its photo-charging characteristics after visible light irradiation, and efficient and sustainable hydrogen production (7.50 μmol cm<sup>-2</sup> in 4 h) in the dark, which realized the desired effect without external power supply, full-day efficient and sustainable hydrogen production. The research work has extended the new application of scPEWFC for simultaneous wastewater treatment and hydrogen production in the dark, and provided some theoretical guidance for developing a novel, sustainable and green energy production routes in environmental and energy field.

### Acknowledgements

This work was financially supported by the National Natural Science Foundation of China (NSFC, No. 21477085, 21537003).

### Notes and references

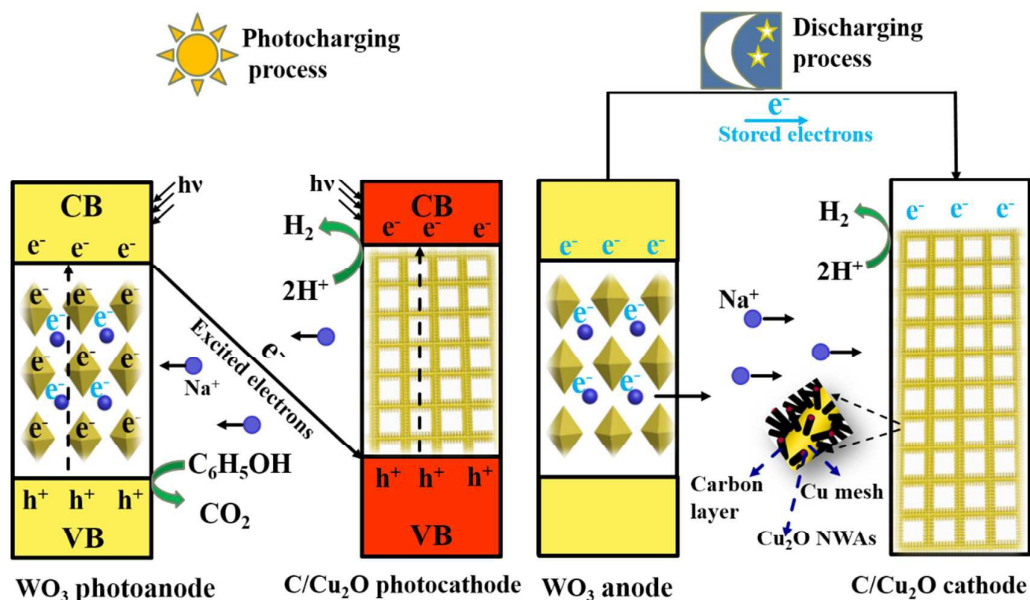
1. I. Ali, *Chemical reviews*, 2012, 112, 5073-5091.
2. C. C. Wang, J. R. Li, X. L. Lv, Y. Q. Zhang and G. Guo, *Energy & Environmental Science*, 2014, 7, 2831-2867.
3. C. Chen, W. Ma and J. Zhao, *Chemical Society Reviews*, 2010, 39, 4206.
4. L. Xia, J. Bai, J. Li, Q. Zeng, X. Li and B. Zhou, *Applied Catalysis B: Environmental*, 2016, 183, 224-230.
5. H. Shi and G. Zhao, *The Journal of Physical Chemistry C*, 2014, 118, 25939-25946.
6. G. Yang, G. Zhang and H. Wang, *Water Research*, 2015, 78, 60-73.
7. M. Gao, L. Zhu, W. L. Ong, J. Wang and G. W. Ho, *Catal. Sci. Technol.*, 2015, 5, 4703-4726.
8. Z. Wu, G. Zhao, Y. Zhang, J. Liu, Y.-n. Zhang and H. Shi, *J. Mater. Chem. A*, 2015, 3, 3416-3424.
9. N. Strataki, M. Antoniadou, V. Dracopoulos and P. Lianos, *Catalysis Today*, 2010, 151, 53-57.
10. Y. Feng, H. Lee, X. Wang, Y. Liu and W. He, *Bioresource Technology*, 2010, 101, 632-638.
11. C. A. Martínezhuitle, M. A. Rodrigo, I. Sirés and O. Scialdone, *Chemical reviews*, 2015, 115, 13362-13407.
12. D. Cambié, C. Bottecchia, N. J. W. Straathof, V. Hessel and T. Noël, *Chemical reviews*, 2016, 116, 10276-10341.
13. A. Rinaldi, B. Mecheri, V. Garavaglia, S. Licoccia, P. D. Nardo and E. Traversa, *Energy & Environmental Science*, 2008, 1, 417-429.
14. Y. Du, Y. Feng, Y. Qu, J. Liu, N. Ren and H. Liu, *Environmental science & technology*, 2014, 48, 7634-7641.
15. B. E. Logan and K. Rabaey, *Science*, 2012, 337, 686-690.
16. W.-W. Li, H.-Q. Yu and Z. He, *Energy & Environmental Science*, 2014, 7, 911-924.
17. Y.-K. Wang, G.-P. Sheng, W.-W. Li, Y.-X. Huang, Y.-Y. Yu, R. J. Zeng and H.-Q. Yu, *Environmental science & technology*, 2011, 45, 9256-9261.
18. W. Yang, K. Y. Kim, P. Saikaly and B. E. Logan, *Energy & Environmental Science*, 2017, 10, 1025-1033.
19. X. Xie, C. Criddle and Y. Cui, *Energy & Environmental Science*, 2015, 8, 3418-3441.
20. H. Wang, F. Qian, G. Wang, Y. Jiao, Z. He and Y. Li, *Acs Nano*, 2013, 7, 8728-8735.
21. Q. Fang, G. Wang and Y. Li, *Nano letters*, 2010, 10, 4686-4691.
22. J. Li, J. Li, Q. Chen, J. Bai and B. Zhou, *Journal of hazardous materials*, 2013, 262, 304-310.
23. B. H. Kim, I. S. Chang and G. M. Gadd, *Appl Microbiol Biotechnol*, 2007, 76, 485-494.
24. Bruce E. Logan, ‡, Bert Hamelers, René Rozendal, II, Uwe Schröder, J. Keller, S. Freguia, P. Aelterman, a. Willy Verstraete and K. Rabaey, *Environmental science & technology*, 2006, 40, 5181-5192.
25. Z. Li, W. Luo, M. Zhang, J. Feng and Z. Zou, *Energy & Environmental Science*, 2013, 6, 347-370.
26. X. Chen, S. Shen, L. Guo and S. S. Mao, *Chemical reviews*, 2010, 110, 6503.
27. M. G. Walter, E. L. Warren, J. R. Mckone, S. W. Boettcher, Q. Mi, E. A. Santori and N. S. Lewis, 2011, 111, 6446-6473.
28. A. Paracchino, V. Laporte, K. Sivula, M. Grätzel and E. Thimsen, *Nature materials*, 2011, 10, 456-461.
29. K. Li, Y. Xu, Y. He, C. Yang, Y. Wang and J. Jia, *Environmental science & technology*, 2013, 47, 3490-3497.
30. K. Li, H. Zhang, T. Tang, Y. Xu, D. Ying, Y. Wang and J. Jia, *Water Research*, 2014, 62, 1-10.
31. Q. Chen, J. Bai, J. Li, K. Huang, X. Li, B. Zhou and W. Cai, *Chemical Engineering Journal*, 2014, 252, 89-94.
32. Y. Liu, J. Li, B. Zhou, X. Li, H. Chen, Q. Chen, Z. Wang, L. Li, J. Wang and W. Cai, *Water Res*, 2011, 45, 3991-3998.
33. G. Ma, T. Hisatomi and K. Domen, *Chemical Society Reviews*, 2014, 43, 7520-7535.
34. Q. Chen, J. Li, X. Li, K. Huang, B. Zhou, W. Cai and W. Shanguan, *Environmental science & technology*, 2012, 46, 11451-11458.
35. H. Tada, T. Mitsui, T. Kiyonaga, T. Akita and K. Tanaka, *Nature materials*, 2006, 5, 782-786.
36. K. Maeda, *Acs Catalysis*, 2013, 3, 1486-1503.
37. P. Zhou, J. Yu and M. Jaroniec, *Advanced Materials*, 2014, 26, 4920-4935.
38. X. L. Yin, L. L. Li, W. J. Jiang, Y. Zhang, X. Zhang, L. J. Wan and J. S. Hu, *ACS Appl Mater Interfaces*, 2016, 8, 15258-15266.
39. X.-L. Yin, G.-Y. He, B. Sun, W.-J. Jiang, D.-J. Xue, A.-D. Xia, L.-J. Wan and J.-S. Hu, *Nano Energy*, 2016, 28, 319-329.
40. C. Ng, Y. H. Ng, A. Iwase and R. Amal, *Applied Materials & Interfaces*, 2013, 5, 5269-5275.
41. S. Higashimoto, T. Shishido, Y. Ohno, M. Azuma, M. Takahashi and M. Anpo, *Journal of the Electrochemical Society*, 2007, 154, F48-F54.
42. C. Ng, A. Iwase, Y. H. Ng and R. Amal, *Journal of Physical Chemistry Letters*, 2012, 3, 913-918.
43. X. Lu, T. Zhai, X. Zhang, Y. Shen, L. Yuan, B. Hu, L. Gong, J. Chen, Y. Gao and J. Zhou, *Advanced Materials*, 2012, 24, 938-944.
44. C. Ng, Y. H. Ng, A. Iwase and R. Amal, *Physical chemistry chemical physics : PCCP*, 2011, 13, 13421-13426.
45. S. N. Lou, N. Yap, J. Scott, R. Amal and Y. H. Ng, *Scientific reports*, 2014, 4, 7428.
46. P. Ngaotranwivat, T. Tatsuma, S. Saitoh, Y. Ohko and A. Fujishima, *Physical Chemistry Chemical Physics*, 2003, 5, 3234-3237.
47. S. Kim and H. Park, *RSC Advances*, 2013, 3, 18424-18429.
48. M. Long, B. Tan, P. Hu, B. Zhou and Y. Zhou, *J. Mater. Chem. A*, 2015, 3, 10195-10198.
49. D. Liu, F. Liu and J. Liu, *Journal of Power Sources*, 2012, 213, 78-82.
50. G. Kim, M. Oh and Y. Park, *Scientific reports*, 2016, 6, 33400.
51. W. Zhao, X.-F. Wang, E. Zheng, Y. Wei, Y. Sanehira and G. Chen, *Journal of Power Sources*, 2017, 350, 28-34.
52. Z. Zhang, R. Dua, L. Zhang, H. Zhu, H. Zhang and P. Wang, *Acs Nano*, 2013, 7, 1709.
53. Y. Chang, K. Yu, C. Zhang, Z. Yang, Y. Feng, H. Hao, Y. Jiang, L. L. Lou, W. Zhou and S. Liu, *Applied Catalysis B Environmental*, 2017, 215.
54. Z. Wu, J. Wang, Z. Zhou and G. Zhao, *J. Mater. Chem. A*, 2017, 5, 12407-12415.
55. R. Levinas, N. Tsyntsaru, M. Lelis and H. Cesiulis, *Electrochimica Acta*, 2017, 225, 29-38.
56. Y. Zhang, B. Tang, Z. Wu, H. Shi, Y. Zhang and G. Zhao, *Green Chem.*, 2016, 18, 2424-2434.
57. X. Lu, S. Xie, H. Yang, Y. Tong and H. Ji, *Chemical Society Reviews*, 2014, 43, 7581-7593.

## ARTICLE

Journal Name

58. Z. Wu, Z. Zhou, Y. Zhang, J. Wang, H. Shi, Q. Shen, G. Wei and G. Zhao, *Electrochimica Acta*, 2017, 254, 140-147.
59. S. Balaji, Y. Djaoued, A. S. Albert, R. Z. Ferguson, R. Brüning and B. L. Su, *Journal of Materials Science*, 2009, 44, 6608-6616.
60. K. Machida and M. Enyo, *Cheminform*, 1990, 137, 1169-1175.
61. C. Santato, M. Odziemkowski, M. Ulmann and J. Augustynski, *Journal of the American Chemical Society*, 2001, 123, 10639-10649.
62. S. Balaji, Y. Djaoued, A. S. Albert, R. Z. Ferguson, R. Brüning and B. L. Su, *Journal of Materials Science*, 2012, 44, 6608-6616.
63. S. H. Lee, M. J. Seong, H. M. Cheong, E. Ozkan, E. C. Tracy and S. K. Deb, *Solid State Ionics*, 2003, 156, 447-452.
64. S. Balaji, A. S. Albert, Y. Djaoued and R. Brüning, *Journal of Raman Spectroscopy*, 2010, 40, 92-100.
65. C. Ng, A. Iwase, Y. H. Ng and R. Amal, *ChemSusChem*, 2013, 6, 291-298.
66. K. A. Newton and F. E. Osterloh, *Topics in Catalysis*, 2016, 59, 750-756.

## Table of Contents Graphic



Solar-charged photoelectrochemical wastewater fuel cell for efficient and sustainable hydrogen production based on the promotion of pollutant oxidation